Atmos. Meas. Tech. Discuss., 7, 5651–5693, 2014
www.atmos-meas-tech-discuss.net/7/5651/2014/
doi:10.5194/amtd-7-5651-2014

Atmospheric Measurement Techniques Discussions

Deployment of a sequential two-photon laser induced fluorescence sensor for the detection of gaseous elemental mercury at ambient levels: fast, specific, ultrasensitive detection with parts-per-quadrillion sensitivity

D. Bauer[1], S. Everhart[1], J. Remeika[1], C. Tatum Ernest[1,*], and A. J. Hynes[1]

[1]Division of Marine and Atmospheric Chemistry, Rosenstiel School of Marine and Atmospheric Science, University of Miami, 4600 Rickenbacker Causeway, Miami, Florida 33149, USA
[*]now at: Atmospheric Chemistry Department, Max Planck Institute for Chemistry, Hahn-Meitner-Weg 1, Mainz, 55128, Germany

Received: 21 May 2014 – Accepted: 22 May 2014 – Published: 6 June 2014

Correspondence to: A. J. Hynes (ahynes@rsmas.miami.edu)

Published by Copernicus Publications on behalf of the European Geosciences Union.

Abstract

The operation of a laser-based sensor for gas phase elemental mercury, Hg(0), is described. It utilizes sequential two photon laser excitation with detection of blue shifted laser induced fluorescence to provide a highly specific detection scheme that precludes detection of anything other than atomic mercury. It has high sensitivity, fast temporal resolution, and can be deployed for in-situ measurements in the open atmosphere with essentially no perturbation of the environment. An ambient sample can also be pulled through a fluorescence cell allowing standard addition calibrations of the concentration. No type of preconcentration is required and there appears to be no significant interferences from other atmospheric constituents including gas phase oxidized mercury species. As a consequence, is not necessary to remove RGM from the air sample. The instrument has been deployed as part of an instrument intercomparison and compares well with conventional instrumentation that utilizes preconcentration on gold followed by analysis using Cold Vapor Atomic Fluorescence Spectroscopy. Currently, the achievable detection sensitivity is $\sim 15\,\mathrm{pg\,m^{-3}}$ ($\sim 5 \times 10^4$ atoms $\mathrm{cm^{-3}}$, ~ 2 ppq) at a sampling rate of 0.1 Hz i.e. averaging 100 shots with a 10 Hz laser system. Preliminary results are described for a 50 Hz instrument that utilizes a modified excitation sequence and has monitored ambient elemental mercury with an effective sampling rate of 10 Hz. Additional work is required to produce the precision necessary to perform eddy correlation measurements. Addition of a pyrolysis channel should allow the measurement of Total Gaseous Mercury, and hence Reactive Gaseous Mercury (by difference) with good sensitivity and time resolution.

1 Introduction

A detailed understanding of the biogeochemical cycling of mercury and the routes to the production of organomercury compounds in ecosystems is a critical issue from a human health perspective. Direct exposure to mercury is primarily through the

AMTD
7, 5651–5693, 2014

ingestion of dimethylmercury from fish consumption, however an understanding of the overall budget and mechanism of chemical transformation of mercury in both its elemental and combined forms is critically important. (US EPA, 2000; Mergler et al., 2007; UNEP, 2008; Diez, 2009). Wet or dry deposition of oxidized mercury is an important step in a complex process that involves both chemistry and microbiology and eventually produces alkyl mercuric compounds. Regulation of anthropogenic mercury sources in the US has almost eliminated emissions from municipal waste combustors and medical waste incinerators and the new "Mercury and Air Toxics Standards" (MATS) will require reductions in mercury emissions from coal burning power plants (US EPA, 2011). On an international scale the United Nations Environment Program has been focused on developing an increased understanding of the global impact of atmospheric mercury (UNEP, 2013). Reductions in mercury emissions have been the focus of global negotiations that have led to the Minimata Convention on Mercury, a multilateral environmental agreement that has been signed by 97 countries (UNEP, 2014). Nevertheless, these developments take place in a situation in which our overall understanding of the chemistry of atmospheric mercury transformation is limited (Hynes et al., 2008; Subir et al., 2011, 2012; Gustin and Jaffe, 2010). In the absence of a detailed understanding of the atmospheric cycling of mercury it is quite possible that the desired environmental results will not be attained. For example, emission controls in the USA are designed to try and reduce the wet and dry deposition that ultimately produces increased mercury concentrations in aquatic environments. If this deposition is controlled by oxidation of the global mercury pool, rather than by US anthropogenic emissions, then emission reductions will not decrease deposition.

The typical background concentrations of Hg(0) in unpolluted environments range from 1.5–2 $\mathrm{ng\,m^{-3}}$ where 1 $\mathrm{ng\,m^{-3}}$ is $\sim 3 \times 10^6$ atoms $\mathrm{cm^{-3}}$ or $\sim$ 120 ppq (parts per quadrillion) and RGM is thought to be typically less than 10 % of this value, hence atmospheric measurements represent a significant challenge in ultratrace analytical chemistry (Gustin and Jaffe, 2010). It is also important to note that the chemical speciation of oxidized mercury has not been established. Current approaches to the measurement

AMTD
7, 5651–5693, 2014

of both elemental and oxidized mercury at ambient levels rely exclusively on instruments that use preconcentration on gold followed by analysis using CVAFS (cold vapor atomic fluorescence spectroscopy). The issues and problems associated with this approach are discussed by Jaffe and Gustin and include the question of the extent to which CVAFS instruments are measuring Hg(0) or TGM or something intermediate between the two. In addition, the necessity to preconcentrate requires a sampling time of minutes for Hg(0) and precludes fast measurements. The current approach to measurement of RGM relies almost exclusively on KCl denuder sampling followed by pyrolysis and CVAFS analysis of the Hg(0) produced by RGM decomposition (Landis et al., 2002).

The development of a fast, in-situ sensor capable of measuring Hg(0) at ambient levels is a critical research need. Such a sensor can independently verify the performance of the CVAFS instruments. In addition, this type of sensor would offer the possibility of measuring mercury fluxes using a direct micro-meteorological approach, the eddy-correlation technique.

We have developed a laser-based sensor for the detection of gas phase elemental mercury, Hg(0), using sequential two-photon laser induced fluorescence (2P-LIF). The instrument is capable of fast, in-situ, measurement of Hg(0) at ambient levels. By incorporating pyrolysis to convert RGM to Hg(0) it is possible to measure total gas phase mercury (TGM) and hence to measure RGM by difference. Under atmospheric conditions the detection of Hg(0) is unambiguous since the sensor can not detect an oxidized mercuric species, irrespective of its chemical speciation, and there are no known atmospheric interferences i.e. atoms or molecules other than Hg(0) that can produce a false positive or artifact signal.

In a prior study we examined four variants of 2P-LIF detection of Hg(0) and performed a detailed laboratory characterization of the spectroscopic characteristics of the most sensitive variant (Bauer et al., 2002, 2003). In this work we describe the performance of a field instrument that uses this approach and was deployed as part of the RAMIX (Reno Atmospheric Mercury Intercomparison Experiment) intercomparison of

AMTD
7, 5651–5693, 2014

mercury detection instruments (Gustin et al., 2013). We also show preliminary results from a "second generation" 2P-LIF system that utilizes a different excitation scheme.

2 Principles of operation

It is instructive to compare the 2P-LIF approach with CVAFS instruments currently used to monitor Hg(0) as exemplified by the Tekran 2537 Mercury Vapour Analyzers (Tekran, 2001). In CVAFS systems, air is pulled through a gold trap that removes gas phase mercury forming an amalgam. After a period of sampling the gold trap is flushed with argon and then heated releasing Hg(0) which flows into a fluorescence cell. A mercury discharge lamp is used to induce fluorescence using the 6^3P_1–6^1S_0 transition at 253.7 nm with detection of resonance fluorescence using a photomultiplier tube. The key features of the instrument are (i) the gold amalgamation step that selectively removes and preconcentrates gas phase mercury; and (ii) the detection of Hg(0) via resonance fluorescence in the presence of an inert gas that does not quench the 6^3P_1 excited state. The removal of air and use of an inert gas is critical for establishing high sensitivity because O_2 is an extremely efficient quencher of the 6^3P_1 excited state. The 6^3P_1 state has a radiative lifetime of 119 ns and the quenching rate coefficient with O_2 is 3.6×10^{-10} cm^3 molecule^{-1} s^{-1} (Michael and Suess, 1974; Breckenridge and Umemoto, 2007). The fluorescence efficiency in air at atmospheric pressure can be calculated using the Stern–Volmer relationship and gives a fluorescence efficiency of 4.7×10^{-3} and an effective radiative lifetime of 0.56 ns. It should be noted that the quenching efficiency of N_2 is approximately two orders of magnitude lower than that of O_2 and that it makes little contribution to quenching in spite of its higher partial pressure (Deech et al., 1971). Commercial instruments utilizing gold amalgamation typically have detection sensitivities of 0.1 ng m^{-3} based on sampling times of 2.5–5 min. It should be clear based on these considerations, that while the CVAFS instrumentation is suitable for ambient monitoring, it is not capable of fast in-situ measurements of Hg(0).

AMTD
7, 5651–5693, 2014

The 2P-LIF instrument utilizes two tunable lasers to sequentially pump two atomic transitions in Hg(0) followed by the detection of blue shifted LIF. The instrument has been deployed in two excitation configurations. In the "first generation" system the first tunable laser operates at a fundamental wavelength of 507.4 nm and is frequency doubled to produce 253.7 nm exciting the Hg 6^3P_1–6^1S_0 transition. This is followed by excitation with a second laser at 407.8 nm to the 7^1S_0 level via the 7^1S_0–6^3P_1 transition. Both radiative decay and collisional energy transfer produce population in the 6^1P_1 level. Blue shifted fluorescence is then observed on the strong 6^1P_1–6^1S_0 transition at 184.9 nm using a solar blind photomultiplier tube. The "second generation" system uses the same Hg 6^3P_1–6^1S_0 transition for the initial excitation and this is followed by excitation of the 6^3D_1–6^3P_1 transition at 313.2 nm. This fluoresces at 579 nm via the 6^3D_1–6^1P_1 transition and again produces population in the 6^1P_1 level. Blue shifted fluorescence is again observed on the strong 6^1P_1–6^1S_0 transition at 184.9 nm using a solar blind photomultiplier tube. The excitation schemes involving sequential excitation of two atomic transitions, followed by detection of the emission from a third are extremely specific and preclude detection of anything other than Hg(0). In typical single photon fluorescence systems, including CVAFS, sensitivity is normally limited by the detection of scattered excitation light that occurs at, or is red shifted relative to the excitation wavelength. 2P-LIF is detected at 184.9 nm with a solar blind photomultiplier tube that has a negligible quantum efficiency beyond 240 nm resulting in no detection of the 407.8 and 313.2 nm excitation scatter and minimal response to the 253.7 nm scatter. This leads to the very high sensitivity. A significant added advantage is that the presence of atmospheric aerosols does not significantly degrade detection sensitivity so it is not necessary to pass the airflow through filters to remove particulates. In systems that utilize resonance fluorescence even a small particulate loading can dramatically degrade sensitivity because of the increase in scattering of the excitation beam. Similarly, detection approaches using CRDS (cavity ring down spectroscopy) require filtering because of the attenuation produced by aerosols. In the sequential two-photon system the increase in scatter of the 253.7 and 407.8 nm beams has little

AMTD
7, 5651–5693, 2014

impact because these wavelengths are not detected by the PMT. In prior work we examined the linearity, saturation and spectroscopic characteristics of the 2P-LIF system using a high power "laboratory" laser system consisting of Nd-Yag laser, dye laser and optical parametric oscillator (Bauer et al., 2002, 2003). Comparison with a Tekran 2537 demonstrated that 2P-LIF is linear over a wide range of Hg(0) concentrations and that the linewidths of the excitation transitions were relatively broad. We also examined the saturation characteristics which show the relationship between the power of the excitation beams and the fluorescence signal. The challenge for the ambient environmental monitoring was to produce a relatively compact laser system that would operate reliably for extended periods of time in a mobile trailer.

3 Description of the mobile instrument

The complete 2P-LIF instrument package deployed for the RAMIX intercomparison was housed in a 20′ × 8′ mobile laboratory. A 4′ × 10′ optic bench supported the laser systems, optics, and sample cells. The system configuration consisted of two dye lasers pumped by a single 10 Hz Nd-YAG laser. The initial excitation and detection scheme, as discussed above, employed one photon each of 253.7 and 407.8 nm light for the sequential excitation of Hg(0) with the detection of fluorescence at 184.9 nm. The third harmonic of the Nd-Yag laser was split and used to simultaneously pump two dye lasers. The first laser, using Coumarin 500 dye, operated at a fundamental wavelength of 507.3 nm and was frequency doubled to produce the 253.7 nm excitation photon. The second dye laser, using Exalite 408 dye, operated at a fundamental wavelength of 407.8 nm, generating the second excitation photon directly. As noted above, the effective radiative lifetime of the 6^3P_1 state is 0.56 ns at atmospheric pressure which is shorter than the excitation pulse duration of ∼ 6 ns. As a consequence the population in the 6^3P_1 essentially tracks the temporal profile of the excitation pulse and accurate synchronization of the excitation pulses is critical. The use of a single pump laser is advantageous because it eliminates the "jitter" associated with the use of two pump

AMTD
7, 5651–5693, 2014

lasers. In practice it was found that a slight delay between the two pulses produces optimal sequential excitation. Hence the two beams were spatially overlapped using dichroic optics, and a delay path ensured the 408 nm pulse arrived 2–3 ns after the 254 nm pulse. In addition, the 254 nm beam passed though a 6x beam expander to reduce the flux and produce better spatial overlap with the 408 nm beam. When sampling in the trailer the combined beams then passed through a sample cell, a reference cell, and then terminated in a beam dump. When the sample cell is utilized, air is pulled through a $1/4''$ o.d. Teflon sampling line with an inlet located above the roof of the trailer. No filters are placed on the inlet. If the ambient temperature is significantly above the trailer temperature and the humidity is high the sample air is passed through a cold trap to prevent condensation on the sampling lines inside the trailer. For open air in-situ sampling on the trailer roof the beams passed through the reference cell and are directed by mirrors though a hole in the trailer roof. The beam then passed between the photocathodes of the two PMTs that were located ~ 3 ft above the trailer roof.

A slow flow of zero grade air passed over a permeation tube located in a temperature controlled oven and provided a stable flow of Hg(0) to the reference cell. The 2P-LIF signal from the sample cell was monitored by two solar-blind PMTs on opposite sides of the sample cell, each aligned perpendicular to the axis of the excitation beams. The 2P-LIF signal from the reference cell was monitored by a single PMT aligned perpendicular to the axis of the excitation beams. The voltage from all three PMTs was amplified and processed by boxcar integrators. Both the single shot and 100 shot exponential average outputs of the boxcar units were digitized and stored in a computer. The detection efficiency of the solar-blind PMTs drops off significantly for wavelengths longer than 200 nm, so no filters were used to discriminate against background trailer light or laser scatter. Scattered laser light was monitored by taking background measurements in which both the 408 and 254 nm beams were blocked giving electronic noise, and then monitoring scatter from both excitation beams separately. Neither PMT saw any scatter from the 408 nm excitation beam. A small amount of 254 nm scatter was observed and so only the 254 nm scatter was routinely monitored. Figures 1 and

AMTD
7, 5651–5693, 2014

2 display 2P-LIF signals monitoring ambient air, as collected by the computer from the boxcar units, the data is a small section of the 1 and 2 September data discussed below. Figure 1 shows the boxcar averaged output for both sample PMTs. The Hg(0) concentration is proportional to the LIF signal detected when both the 254 and 408 nm beams are present minus the 254 nm scatter signal and the absolute concentration scale has been calibrated as discussed below. The electronic noise and 254 nm scatter are labeled in Fig. 1 and it can be seen that the sensitivity of the PMTs to 254 nm scatter is different with tube B seeing significantly more scatter. The voltage and hence the gain of the PMTs was adjusted to optimize the sensitivity and dynamic range of the 2P-LIF signal however tube B had higher gain and required more frequent adjustment. All data was processed to account for the varying amplification of the PMTs, then background subtracted.

In Fig. 2 a 180 s slice of data shows the 1 s average of the 10 Hz single shot data together with the exponentially averaged output of the boxcar and a 7 s smoothing of the single shot data. The agreement between the digitally averaged single shot data and the analogue boxcar average is excellent. It shows that a nominally 100 shot exponential average is essentially equivalent to a 7 s smoothing of the single shot data.

Either a Tekran 2537A or 2537B mercury analyzer was located downstream from the sample cell and sampled 2 SLPM from the gas flow. The Tekran sampled through a 1μ Teflon particle filter but no additional filters were used. A mass flow controller and diaphragm pump located downstream from the Tekran pulled an additional 8 SLPM of air so that the total flow through the sampling cell was 10 SLPM. The sample cell was connected to the RAMIX manifold by $1/4''$ Teflon tubing. The sample air could be routed through a second temperature controlled permeation oven that contained a low output permeation tube. The temperature was set to produce an addition of typically 5 ng m^{-3} of Hg(0) above ambient, as measured by the Tekran 2537. We fabricated both permeation ovens and the permeation tubes. The actual sampling configurations evolved over the course of the campaign and the appropriate specific sampling configurations are described in the results sections.

AMTD
7, 5651–5693, 2014

The instrument has been deployed in Miami, FL and Reno, NV and in both places the ambient temperature was well in excess of 30 °C during the day. It was critical to keep the internal trailer temperature at a constant temperature close to 20 °C to ensure stable operation of the laser systems hence the trailer had three ac units installed.

3.1 Hg concentration units

It has become standard practice in the mercury community to report Hg(0) concentrations in ng m^{-3} referenced to 1 standard atmosphere and 0 °C as these are the concentrations reported by the Tekran 2537 units, irrespective of the actual sampling pressure and temperature. As a consequence, these units rather than being absolute concentrations effectively report mixing ratios and a knowledge of the sampling pressure and temperature is required to convert these "mixing ratios" to absolute concentrations. In this paper we will retain this convention using ng m^{-3} referenced to 1 standard atmosphere and 0 °C unless clearly specified otherwise.

3.2 Reference normalization

At the start of a measurement cycle the excitation dye lasers were optimized to produce the maximum 2P-LIF signal by maximizing output power and then tuning the wavelengths to generate the maximum 2P-LIF signal. At this point the laser wavelengths should be centered on the Hg(0) absorption features and the 2P-LIF signal will be proportional to the Hg(0) concentration. In practice both the wavelength and power of the excitation lasers can drift and the 2P-LIF signal will no longer be proportional to the Hg(0) concentration. The power will decrease as the laser dyes degrade and wavelengths can drift as a result of temperature variation and problems with mechanical stability. This is a particular challenge in a mobile laboratory. At the excitation powers used in these experiments the two atomic transitions are partially saturated and there is no simple relationship between the 2P-LIF signal and the laser powers. Small drifts in wavelength are also difficult to monitor and correct for. To compensate for these drifts,

AMTD
7, 5651–5693, 2014

the 2P-LIF signal was monitored in a reference cell that maintained a constant concentration of Hg(0). Any drifts in power or wavelength were then observed as a change in the 2P-LIF signal from the reference cell. The 2P-LIF signal from the sample cell was then normalized to this reference signal. Figure 3 shows the 2P-LIF signal from the reference cell from 26 h of continuous measurement on 1 and 2 September. The reference 2P-LIF signal, which should be constant if the lasers showed no drift, shows fluctuations of 20 % over the first 15 h and then a precipitous drop in power as the dyes degrade. At hour 25, ∼ 1 a.m. on 2 September, the dyes were changed and the power restored. The reference cell signal also provides a long term monitor of the performance of the laser and detection systems. All of the data from ambient samples were background corrected and then normalized to the reference cell.

3.3 Calibration

Laser induced fluorescence is a relative technique since it is not possible to accurately relate the fluorescence signal measured by the PMT to the absolute concentration of the species being monitored. As a consequence it must be independently calibrated by standard addition of a calibration gas or by comparison with another absolute technique. The 2P-LIF system was calibrated by reference to the Tekran 2537 that was sampling simultaneously from the gas flow. Typically the integrated 2P-LIF signal was referenced to 15 min of Tekran sampling during each measurement period and the response of both instruments was compared over the whole measurement period. The Tekran 2537 utilizes a built in, gravimetrically calibrated, Hg(0) permeation tube to calibrate the CVAFS fluorescence signal. Ambient concentrations and spikes were being simultaneously monitored by several Tekran 2537 units and these experiments will be described in detail elsewhere. In addition a spike in the Hg(0) concentration was introduced using the inline permeation oven and the Tekran and 2P-LIF responses were compared.

AMTD
7, 5651–5693, 2014

3.4 Instrument response and linearity

The instrument response and linearity of an LIF sensor are dependent on quenching or absorption of the fluorescence signal by atmospheric gases. The Hg 6^3P_1 state that is excited in the first step of the 2P-LIF scheme is quenched very efficiency by O_2 but data on the quenching efficiency of the higher electronic states that are subsequently excited prior to fluorescence is limited. Nevertheless it is reasonable, based on 6^3P_1 quenching rates, to conclude that at atmospheric pressure 2P-LIF fluorescence efficiency is low. In addition, the 184.9 nm fluorescence signal is absorbed by both O_2 and H_2O. The absorption cross sections of O_2 and H_2O are $\sim 1 \times 10^{-20}$ and 7×10^{-20} cm^2 $molecule^{-1}$, respectively (Creasey et al., 2000). The path length from the 2P-LIF beams to the PMT photocathode is ~ 3 cm which means that the 184.9 nm bean is attenuated by ~ 15 % by O_2 at atmospheric pressure and by 0.7 % per Torr of H_2O. If both the pressure and gas composition are constant then both the fluorescence efficiency and the attenuation of the 2P-LIF are constant and the 2P-LIF signal should be proportional to the Hg(0) concentration. If gas composition or pressure are changing significantly this could produce deviations from linearity. This is a significant issue in the use of LIF in reactive flows such as combustion or plasma environments and it could be significant in an aircraft deployment. For ground based measurements the pressure is constant and the only potential issue is a change in the H_2O partial pressure. We performed linearity calibrations employing the mobile laser system and using standard addition to air. We also estimated the effective fluorescence efficiency in our experimental configuration by measuring the relative fluorescence yields in air and He and we examined the effects of changes in H_2O concentration on the 2P-LIF fluorescence response.

2P-LIF linearity in air

These experiments used an experimental configuration that was identical to that used during the RAMIX intercomparison to compare the 2P-LIF signal with Hg(0) concentrations measured by the Tekran 2537B. A constant flow of zero grade air passed through

AMTD
7, 5651–5693, 2014

a temperature controlled aluminum oven containing a Teflon mercury permeation tube, supplying a constant amount of Hg(0) into the air stream. The flow was controlled by a mass flow controller (MFC). An additional flow of air, controlled by a separate MFC, bypassed the permeation tube and was then added to the perm oven flow in a mixing line to dilute the Hg(0) concentration and provide variable concentrations for study. Another MFC, backed by a mechanical pump, downstream of the LIF sample cell, ensured a constant 5.0 SLPM flow through the LIF sample cell (including air flow sampled by the Tekran), while a vent line open to ambient atmosphere upstream of the sample cell kept the entire sampling system at atmospheric pressure. The simultaneous detection of Hg(0) using LIF and Tekran measurements was conducted over a range of 3–18.5 ng m^{-3} by varying the air flow through the dilution line. There is an excellent correlation between the 2P-LIF signal and the Tekran measurements, as shown in Fig. 4 with a least-squares linear regression of the data giving an R^2 of 0.996 and an intercept of 0.06 ± 0.1, i.e. zero within the precision of the measurement. The experiment was then repeated with higher Hg(0) concentrations (12.5–30 ng m^{-3}), and again, there was an excellent linear correlation between the LIF signal and the Tekran measurements; $R^2 = 0.998$ and a zero intercept at a 2σ level of precision. In both cases the variations in concentration were in excellent agreement with those calculated based on the measured dilution. These results verify our prior work in N_2 using the "field instrument" configuration and confirm that, as expected, at constant pressure the 2P-LIF signal varies linearly with Hg(0) concentration in air.

The relative fluorescence efficiencies in air and He were measured by passing both gases through the permeation oven that was used for standard addition of Hg(0) to sample gases. In this case zero grade air or He was used and the 2P-LIF signal was monitored in each case. The average of these experiments gave a 2P-LIF signal in air that was 3 % of the signal in He. Approximately 15 % of the reduction in signal is due to direct absorption of the 2P-LIF signal by O_2 and the remaining reduction is probably due to enhanced quenching by O_2. Assuming the maximum possible 100 % in He as an example, we would obtain a fluorescence efficiency of approximately 3.5 % in air.

AMTD
7, 5651–5693, 2014

As noted above in the low laser power linear fluorescence regime we would expect a fluorescence efficiency of less than 0.5 %. While the fluorescence efficiency in He is probably less than 100 % it is expected to be high. As shown previously, at the typical powers and laser fluxes used here both excitation transitions are partially saturated and this is likely to explain the higher fluorescence efficiency.

The impact of water vapor was measured by pulling outside air through a water bubbler and measuring the 2P-LIF signal as a function of humidity. Relative humidity was monitored using a humidity sensor and the absolute concentration of water was calculated using the trailer temperature. Figure 5 shows the 2P-LIF signal as a function of water concentration and it can be seen that the signal drops as the concentration increases. As noted above we expect a decrease in the 2P-LIF signal as a result of absorption by the water vapor but the observed decrease, shown in Fig. 5 as the "exp" line, is larger than calculated due to absorption alone. There is no literature data on the quenching of excited states of Hg(0) by water but this result suggests it is also an extremely efficient quencher and this requires further investigation. Typically the H_2O partial pressure is constant over extended periods of time and the diurnal change in relative humidity is a consequence of temperature change. Nevertheless we plan to incorporate a humidity measurement downstream of the Tekran and routinely monitor the H_2O partial pressure.

4 Interference effects

As we noted above, the 2P-LIF excitation schemes, involving sequential excitation of two atomic transitions followed by detection of the emission from a third, are extremely specific and preclude detection of anything other than atomic mercury. However it is possible to conceive of interferences, i.e. spurious effects that produce a 2P-LIF Hg(0) signal that does not come from ambient Hg(0). Examples of such interferences include photochemistry coupled with chemistry, the classic example in atmospheric chemistry being the O^1D interference in monitoring ambient OH (Heard and Pilling, 2003). In this

AMTD
7, 5651–5693, 2014

case, excitation of OH on the A-X (1-0) band photodissociates O_3 generating O^1D that reacts with water vapor generating OH. Because of the concentration of water vapor in the lower atmosphere and the very fast rate coefficient for this reaction, a single 282 nm laser pulse can generate O^1D and detect the OH product and this essentially precludes this approach to monitoring tropospheric OH. In the 2P-LIF detection approach the 253.7 nm laser will dissociate ozone and while most of the O^1D produced will be collisionally relaxed to O^3P followed by recombination to reform O_3, a small fraction will react with water to form OH. The reaction of Hg(0) with OH is very slow and this will not have any impact on the 2P-LIF measurements (Bauer et al., 2003).

The second type of interference is a purely photochemical interference in which the probe laser photodissociates a parent molecule, producing, as a photofragment, the molecule or atom under study. An example of such an interference appeared in early attempts to monitor H atoms in flames using 2-photon excitation at 205 nm (Goldsmith, 1986). It became clear that the 2-photon LIF signal did not reflect the nascent H atom concentrations in the flames but was in fact produced by the photodissociation of water vapor. Photolysis of oxidized mercury compounds such as $HgCl_2$ and $HgBr_2$ can produce some Hg(0) photofragments however the absorption cross section for Hg(0) is approximately three orders of magnitude greater than that of HgX_2 compounds at 253.7 nm and under ambient conditions the concentration of HgX_2 is normally much lower than Hg(0) (Templet et al., 1972; Maya, 1977). We will discuss the interference tests conducted during RAMIX campaign elsewhere but it should be noted that there are no potential effects in monitoring ambient Hg(0). This is not necessarily the case in reacting combustion flows, in an environment in which most of the mercury is present as Hg(II) the photochemical interference could become significant.

AMTD
7, 5651–5693, 2014

5 Results

5.1 General overview

For the RAMIX intercomparison the mobile lab was towed from Miami to Reno, a 3000 mile journey, in August 2011. After arrival in Reno it took approximately 3 days to hook up utilities, set up the lab and begin taking data. For most of the intercomparison we sampled from the RAMIX manifold that was designed to allowed simultaneous sampling by the four RAMIX participants and also by the University of Nevada, Reno (UNR) host group. The manifold is described in detail by Finley et al. (2013). During the RAMIX campaign we sampled on 18 days, typically sampling for between 4 and 6 h. The longest period of continuous sampling lasted for 26 h and occurred on 1 and 2 September. Over this 18 day period we sampled from the RAMIX manifold and, in addition at the end of the campaign we sampled ambient air independently and also attempted to measure RGM by pyrolyzing the sample air and measuring the difference between Hg(0) and TGM. During this period the ambient air sampled by the RAMIX manifold was spiked with additional known concentrations of Hg(0), RGM, H_2O, and O_3 both separately and concurrently. The RAMIX results, including a detailed comparison with multiple Tekran instruments, the interference tests and the preliminary attempts to measure RGM will be described elsewhere. Here we focus on the overall instrument performance, derived limits of detection and, in addition the preliminary results from 10 and 50 Hz system utilizing the 313.2 nm, 6^3D_1–6^3P_1 transition for the second excitation photon.

5.2 Extended sampling

The quality of the data during an extended operation can be gauged from data obtained on 1 and 2 September when we were able to perform 26 h of continuous sampling. Figures 6 and 7 show the full sampling period that began shortly before 10 a.m. on 1 September. The *x* axis shows the hour after midnight on 31 August in local time in

AMTD
7, 5651–5693, 2014

Reno and the y axis shows the measured concentrations in ng m^{-3} as measured by the Tekran 2537B. Since the 2P-LIF measurement gives a relative response we have normalized the 2P-LIF signal to the Tekran readings at hour 13.1, shortly after 1 p.m. on 1 September. The Tekran signal is a 2.5 min average, the LIF signals are the average of the boxcar outputs, effectively a 7 s average of 10 Hz data and a 3 min smoothing of that data that makes it easier to track the differences between the Tekran and LIF signals. The LIF signals from each PMT has been corrected for laser background, and changes in gain when PMT voltages were adjusted and then normalized to changes in the reference cell signal. The average of these two background corrected signals was then taken. Figure 7 shows the full sampling record for the 26 h sampling period but with an expanded concentration scale. We began taking data shortly before 10 a.m. and saw the 10 a.m. elemental mercury spike that was added to the RAMIX manifold. At hour 33, corresponding to 9 a.m. on 2 September we also saw the manifold spike and shortly after we stopped sampling from the manifold. The expanded concentration scale in Fig. 7 shows the ambient air signal more clearly and we see a diurnal variation in the Hg(0) concentration that is captured in both the 2P-LIF and Tekran data. Figures 6 and 7 show that there are issues in the scaling of the signals and that the 2P-LIF and Tekran signals are not responding in an absolutely linear fashion with respect to each other. There is a significant discrepancy in the magnitude of the manifold spikes and, at least for the initial spike, the instability in the lasers during this startup period is reflected in the reference cell signal. In addition we had significant problems with the response and calibration of the Tekran 2537B that we suspect are due to the large drop in pressure between the manifold and sampling cell. For this dataset we find that calibrating the 2P-LIF signal using the UNR Tekran data at the second spike produces better agreement over the 26 h sampling period. In the figures the gaps in the LIF signal correspond to, typically, 3 min gaps when laser background signals were recorded. In these plots these periods were set equal to zero. If we examine a 5 h period during the night we see significant fluctuations that are captured by both the LIF and Tekran instruments however the concentration scaling is an issue. Figure 8

AMTD
7, 5651–5693, 2014

shows the LIF data rescaled to the Tekran concentration at a concentration peak that occurs shortly before hour 26.2 on 2 September, we see reasonable but certainly not perfect agreement in the fluctuations in Hg(0) concentration. As noted above, we see better agreement over the 26 h sampling period if we normalize to the UNR Tekran. On 5 September the LIF instrument sampled for seven hours and on this day there was excellent agreement between three independently operated Tekran instruments and the normalized LIF signal including two large manifold Hg(0) spikes. We will address the issues of variability between the Tekran and LIF instruments elsewhere. Nevertheless we conclude that both instruments are clearly measuring Hg(0).

The 2P-LIF instrument shows short term temporal variations in Hg(0) concentration and it is important to determine how much of the short term temporal variation is "real", i.e. it reflects actual short-term variation in the Hg(0) concentration, how much is a reflection of statistical noise in the LIF signal, and how much is an instrumental artifact. This is important in evaluating the RAMIX dataset and critical in evaluating the feasibility of eddy correlation measurements with this system. Ideally we could assume that features that are correlated between the two PMT's reflect a real variation in the Hg(0) signal however the difference in the susceptibility to the 253 nm scatter makes this somewhat problematic. Figure 9 shows a greatly expanded scale capturing 10 min of continuous sampling at hour 13. This is the section of the dataset that was used to calibrate the 2P-LIF signals for the whole 26 h period by normalizing the integral of the 10 min 2P-LIF signals to the Tekran concentration. The figure shows the two individual boxcar outputs, i.e. 7 s averages of the 10 Hz signals. Figure 10 shows the average of the two signals and the reference cell output normalized to the same amplitude as PMTs A and B. It is apparent that there are fluctuations on a 7 s timescale that are captured by both LIF PMTs but some of the fluctuations are not correlated. Comparison with the reference cell output shows that the variation in the ambient LIF signal is not due to pulse-to-pulse or short term wavelength variations in the probe lasers. In fact the mean of the normalized signals is 1.7 ng m^{-3} and the 1σ variation in the signals is 0.18, 0.17 and 0.03 ng m^{-3} for PMT A, PMT B and the reference PMT,

AMTD
7, 5651–5693, 2014

respectively. In contrast the 1σ variation in the 253 nm scatter is 0.012 ng m^{-3} for PMT A and 0.071 ng m^{-3} for PMT B. Based on this we might conclude that the fluctuations we see in the PMT A signal are real however we know that the quantum efficiency of the solar blind PMTs are very low, ~ 0.1 %, and so we do not detect many photons per shot. The shot noise associated with sampling 70 laser pulses would be ~ 12 % detecting 1 photon per pulse and ~ 2 % detecting 25 photons per pulse. This is the 1σ deviation in the magnitude of the signal that is assumed to be proportional to the number of photons detected. Hence it seems reasonable that at least some of the uncorrelated variation in the ambient Hg(0) signals from PMTs A and B are likely to be a result of photon statistics.

5.3 Permeation oven calibrations

Figure 11 shows data from 8 September when we attempted an in-situ calibration using permeation oven additions. On this day there were additional manifold spikes of Hg(0) at ~ 9 and 14 h and also ongoing manifold spikes of water and $HgBr_2$. In Fig. 11 the manifold spikes are labeled as 1 and 6 and the agreement between the values reported by the UM, UW and UNR Tekrans was good. The inline Hg(0) additions are labeled as 2, 3, 4 and 5. The figure shows a comparison of the 2P-LIF and Tekran data with the 2P-LIF signal normalized to manifold addition 1 at ~ 9 a.m. It can be seen that over the course of the six hours of sampling that the 2P-LIF signal is drifting upward relative to the Tekran output. The integrated additions from the Tekran give an average addition of 9.7 ng m^{-3} for peak 2, rising to 10.3 ng m^{-3} for peak 5 and the concentrations for peaks 1 and 6 agree well with the other independent Tekran measurements. This suggests that the oven is not completely stable with an output that rises by ~ 6 % over three hours. It also implies that the discrepancy between the measurements is a result of problems with the 2P-LIF system. A closer examination of the 2P-LIF signal shows that the upward divergence is a result of the normalization procedure i.e. a significant drop in the reference cell signal. We also found that there is some drift in the individual

AMTD
7, 5651–5693, 2014

channels i.e. the individual PMT outputs. This could be a result of problems with one or both of the PMTs or the cell windows but is more likely due to drifts in the signal processing electronics and we need to examine this in more detail.

5.4 Trailer rooftop sampling at RAMIX

On the final day of the RAMIX experiment we sampled directly on the trailer roof, placing a PMT approximately three feet above the trailer roof. The laser beams were directed through the sampling and reference cells within the trailer and were reflected vertically passing through a hole in the trailer roof. The sample cell in the trailer was switched between a sample line located on the roof next to the roof PMT and the RAMIX manifold. This enabled us to simultaneously sample the air above the trailer directly and using a sampling line and sample cell. It is worth noting that the PMTs require no type of filter, hence the roof PMT had the excitation laser beams passing directly in front of the bare photocathode that was directly exposed to both laser scatter and sunlight.

The PMT on the sample cell was approximately 5 cm from the excitation lasers, constrained by the length of the sample cell side arms. Since the number of photons collected varies inversely as the square of the distance of the photocathode from the excitation beams there is a significant advantage in working in ambient air with no sample cell. Firstly, there is an increase in signal because the cell is closer to the excitation beam. Secondly, there is no 254 nm scatter from the cell windows. Figure 12 shows a comparison of the LIF signals from the PMTs on the roof and in the sample cell. The signals are normalized to the Hg(0) concentration measured by the Tekran after the sample cell. The fluctuations in the LIF signal from roof PMT are significantly smaller than the fluctuations in the cell PMT. This is consistent with the conclusion that these fluctuations are related to the limited number of photons collected.

AMTD
7, 5651–5693, 2014

5.5 2P-LIF using excitation of the 6^3D_1–6^3P_1 transition

In an effort to increase the fluorescence photon flux we have investigated an alternate excitation scheme in which we pump the 6^3D_1–6^3P_1 transition at 313.2 nm as the second step in sequential excitation. The 6^3D_1 level then fluoresces via the 6^3D_1–6_1P_1 transition at 579.0 nm, populating the 6^1P_1 level. As before, we monitor fluorescence from the 6^1P_1–6^1S_0 transition at 184.9 nm. The experiment is similar to that described previously, however we now use the residual second harmonic of the Nd-Yag laser to pump a dye laser operating with DCM dye ~ 626 nm. The 626 nm is then frequency doubled in a KPD crystal producing the 313.2 nm excitation photon. This scheme allows us to use the additional residual power at 532 nm that is not utilized in the first excitation configuration but it requires frequency doubling the second dye laser. Figure 13 shows an example of data collected on the Rosenstiel School campus with the trailer located next to the campus dock. The PMTs are located on the trailer roof so no sampling cell is used. The air close to the PMTs was sampled using the Tekran to put the 2P-LIF signals on an absolute concentration scale. The data was obtained using the 10 Hz Nd-Yag laser to pump the dye lasers. Figure 14 has an expanded x axis showing a one-minute segment of the data and includes the individual PMT outputs and their average with the time axis in seconds. It can again be seen that an examination of the correlation between the 2P-LIF signals from two PMTs is useful in seeing the difference between real fluctuations in the Hg(0) concentration and noise from photon statistics. For example it is clear that the feature at 16:55:26 showing an ~ 3 ng m^{-3} spike in the Hg(0) concentration is real. This feature has a width at half maximum of ~ 3 s and again demonstrates the ability of the instrument to capture a very rapid fluctuations in Hg(0) concentration at ambient levels. We never saw this type of fluctuation during RAMIX and these observations, with a location close to the RSMAS dock overlooking Biscayne Bay are interesting.

Figure 15 gives an example of the current performance of the 50 Hz system, taking 5 shot averages to give an effective sampling time of 10 Hz.

AMTD
7, 5651–5693, 2014

The figure shows a 5 s slice of data giving the outputs of PMT A, PMT B, their average and the reference cell. We see rapid variation in the ambient signal that is not present in the reference cell signal indicating that these fluctuations are not due to instrumental artifacts. However we again see that some of the fluctuations are not correlated between the two tubes suggesting that the fluctuations are, at least in part, a reflection of the photon statistics. We believe that a significant increase in the power of the 313 nm excitation beam is possible and that we can also increase the number of detection PMTs to increase the number of photons collected and improve the photon statistics.

5.6 Detection sensitivity

We have used the 254/408 nm detection at 10 Hz and the 254/313 nm excitation scheme with both the 10 and 50 Hz laser systems. The use of the 50 Hz system in the mobile laboratory is somewhat more challenging because of the sensitivity of the Nd-Yag pump laser to temperature fluctuations. In addition, we have a relatively limited experience in the use of the PDL dye lasers with 50 Hz pumping and we saw a very large decrease in the output power at 313 nm as compared to the decrease at 254 nm. Table 1 shows an example of the limits of detection (LODs) that we have achieved examining the 10 Hz data from RAMIX with 245/408 nm excitation and using both 10 and 50 Hz pump lasers with the 254/313 nm excitation scheme with the mobile laboratory located at RSMAS close to Biscayne Bay. The analysis examined blocks of data that were taken contiguously with typically 5–10 min of signal with one minute of background sampling before and after. The LOD is a two-sigma measure of the standard deviation in the background scatter. The limits of detection we have achieved with the 313 nm scheme are comparable to those achieved using 408 nm. As a practical matter the advantages associated with the use of a red dye in methanol solution with a long lifetime compared with the use of an exalite dye in dioxane solution are significant and outweigh the disadvantage of having to frequency double. The detection limits we have achieved after a relatively short period of time are comparable to those achieved with

AMTD
7, 5651–5693, 2014

the 408 nm system after several years of development. At the moment the large drop in 313 nm power associated with the switch to 50 Hz pumping is significantly limiting our detection sensitivity and we expect to achieve a considerable gain in sensitivity if we can improve the 313 nm output.

6 Measurement of total gaseous and reactive gaseous mercury

It is worth noting that the detection sensitivities achieved here suggest that adding a second analysis cell and using pyrolysis to measure total gaseous mercury (TGM) could allow us to measure RGM by difference with sufficiently high sensitivity to make ambient measurements if we average for 30 s. We made some preliminary measurements of TGM using pyrolysis during RAMIX and these measurements will be described elsewhere.

7 Comparison with other techniques

As noted above CVAFS techniques are currently the standard approach to the measurement of Hg(0) and TGM. As has been discussed elsewhere, the extent to which CVAFS systems measure some fraction of RGM is an issue that requires resolution. However it is clear that these systems require preconcentration and are not capable of fast in-situ determination of Hg(0). Pierce et al. (2013) provide a review of CRDS and other mercury sensors that might offer an alternative to CVAFS. Fain et al. (2010) proposed that CRDS is capable of fast in-situ measurements and reported a detection sensitivity of 0.1 ng m^{-3} with a 10 s time resolution. In more recent work, the same group appears to have acknowledged that in-situ measurements of Hg(0) are not feasible using CRDS and that the sample needs to be stripped of ozone before introduction into the CRDS cavity (Pierce et al., 2013). Under these conditions they report a detection sensitivity of 0.35 ng m^{-3} with an integration time of 5 min. The ozone is stripped from the ambient sample by pyrolysis which will certainly convert RGM to Hg(0) so any

AMTD
7, 5651–5693, 2014

RGM must be removed before pyrolysis. It appears that the CRDS technique is not capable of the sensitivity and time resolution currently achievable with CVAFS instruments and it is unlikely to be useful for fast in-situ measurements of Hg(0) at typical ambient levels.

8 Conclusions

We have described the deployment of a laser-based sensor for gas phase elemental mercury that has high sensitivity and fast temporal resolution. The sensor can be deployed for in-situ measurements in the open atmosphere with essentially no perturbation of the environment. An ambient sample can also be pulled through a fluorescence cell allowing standard addition calibrations of the concentration. No type of preconcentration is required and there appears to be no significant interferences from other atmospheric constituents including gas phase oxidized mercury species. As a consequence, is not necessary to remove RGM from the sample. Currently achievable detection sensitivity is $\sim 15\,\mathrm{pg\,m^{-3}}$ ($\sim 5 \times 10^4$ atoms $\mathrm{cm^{-3}}$, ~ 2 ppq) with a 10 s detection time. The instrument has operated with an effective time resolution of 10 Hz but additional work is required to produce the precision necessary to perform eddy correlation measurements. Addition of a pyrolysis channel should allow the measurement of TGM, and hence RGM (by difference) with good sensitivity and time resolution.

Acknowledgements. This work was supported by a National Science Foundation Major Instrumental Grant (#MRI-0821174), by NSF Grant # AGS-1101965 and by the Electric Power Research Institute. We thank Mae Gustin and her research group for their hospitality and assistance during the RAMIX intercomparison.

AMTD
7, 5651–5693, 2014

References

Bauer, D., Campuzano-Jost, P., and Hynes, A. J.: Rapid, ultra-sensitive detection of gas phase elemental mercury under atmospheric conditions using sequential two-photon laser induced fluorescence, J. Environ. Monitor., 4, 339–343, 2002.

Bauer, D., D'Ottone, L., Campuzano-Jost, P., and Hynes, A. J.: Gas phase elemental mercury: a comparison of LIF detection techniques and study of the kinetics of reaction with the hydroxyl radical, J. Photochem. Photobio, 57, 247–256, doi:10.1016/S1010-6030(03)00065-0, 2003.

Breckenridge, W. H. and Umemoto, H.: Collisional quenching of electronically excited metal atoms, in: Advances in Chemical Physics: Dynamics of the Excited State, Vol. 50, edited by: Lawley, K. P., John Wiley & Sons, Inc., Hoboken, NJ, USA, doi:10.1002/9780470142745.ch5, 2007.

Creasey, D. J., Heard, D. E., and Lee, J. D.: Absorption cross-section measurements of water vapour and oxygen at 185 nm, implications for the calibration of field instruments to measure OH, HO_2 and RO_2 radicals, Geophys. Res. Lett., 27, 1651–1654, doi:10.1029/1999GL011014, 2000.

Deech, J. S., Pitre, J., and Krause, L.: Quenching and depolarization of mercury resonance, Can. J. Phys., 49, 1976–1981, 1971.

Diìez, S.: Human health effects of methylmercury exposure, environ, Rev. Environ. Contam. T., 198, 111–132, doi:10.1007/978-0- 387-09646-9, 2009.

Faïn, X., Moosmüller, H., and Obrist, D.: Toward real-time measurement of atmospheric mercury concentrations using cavity ring-down spectroscopy, Atmos. Chem. Phys., 10, 2879–2892, doi:10.5194/acp-10-2879-2010, 2010.

Finley, B. D., Jaffe, D. A., Call, K., Lyman, S. N., and Gustin, M.: Development, testing, and deployment of an air sampling manifold for spiking elemental and oxidized mercury during RAMIX, Environ. Sci. Technol., 47, 7277–7284, doi:10.1021/es304185a, 2013.

Goldsmith, J. E. M.: Photochemical effects in 205 nm, two photon-excited fluorescence detection of atomic hydrogen flames, Opt. Lett., 11, 416–418, 1986.

Gustin, M. and Jaffe, D.: Reducing the uncertainty in measurement and understanding of mercury in the atmosphere, Environ. Sci. Technol., 44, 2222–2227, 2010.

Gustin, M. S., Huang, J., Miller, M., Peterson, C., Jaffe, D., Ambrose, J., Finley, B., Lyman, S., Call, K., Talbot, R., Feddersen, D., Mao, H., and Lindberg, S.: Do we understand what the

AMTD
7, 5651–5693, 2014

mercury speciation instruments are actually measuring? Results of RAMIX, Environ. Sci. Technol., 47, 7295–7306, doi:10.1021/es3039104, 2013

Heard, D. E. and Pilling, M. J.: Measurement of OH and HO_2 in the troposphere, Chem. Rev., 103, 5163–5198, 2003

Hynes, A. J., Donohoue, D. L., Goodsite, M. E., and Hedgecock, I. M.: Our current understanding of major chemical and physical processes affecting mercury dynamics in the atmosphere and at the air-water/terrestrial interfaces in mercury fate and transport in the global atmosphere, edited by: Mason, R. and Pirrone, N., Spring, New York, NY, 2009.

Landis, M. S., Stevens, R. K., Schaedlich, F., and Prestbo, E. M.: Development and characterization of an annular denuder methodology for the measurement of divalent inorganic reactive gaseous mercury in ambient air, Environ. Sci. Technol., 36, 3000–3009, 2002.

Maya, J.: Ultraviolet absorption cross sections of HgI_2, $HgBr_2$, and tin(II) halide vapors, J. Chem. Phys., 67, 4976, doi:10.1063/1.434681, 1977.

Mergler, D., Anderson, H. A., Chan, L. H. M., Mahaffey, K. R., Murray, M., Sakamoto, M., and Stern, A. H.: Methylmercury exposure and health effects in humans: a worldwide concern, Ambio, 36, 3–11, 2007.

Michael, J. V. and Suess, G. N.: Absolute Quenching Cross-Sections of Hg (^{3}P) with various molecules, J. Phys. Chem., 78, 482–487, 1974.

Pierce, A., Obrist, D., Moosmüller, H., Faïn, X., and Moore, C.: Cavity ring-down spectroscopy sensor development for high-time-resolution measurements of gaseous elemental mercury in ambient air, Atmos. Meas. Tech., 6, 1477–1489, doi:10.5194/amt-6-1477-2013, 2013.

Subir, M., Ariya, P. A., and Dastoor, A. P.: A review of uncertainties in atmosphericmodeling of mercury chemistry I. Uncertainties in existing kinetic parameters: fundamental limitations and the importance of heterogeneous chemistry, Atmos. Environ., 45, 5664–5676, 2011.

Subir, M., Ariya, P. A., and Dastoor, A. P.: A review of the sources of uncertainties in atmospheric mercury modeling II. Mercury surface and heterogeneous chemistry – a missing link, Atmos. Environ., 46, 1–10, 2012.

Tekran: Model 2537A Mercury Vapour Analyzer User Manual, Tekran Inc., Toronto, Ontario, 2001.

Templet, P., McDonald, J. R., McGlynn, S. P., Kendrow, C. H., Roebber, J. L., and Weiss, K.: Ultraviolet absorption spectra of mercuric halides, J. Chem. Phys., 56, 5746, doi:10.1063/1.1677111, 1972.

AMTD
7, 5651–5693, 2014

UNEP: United Nations Environment Program, Chemicals Branch, The Global Atmospheric Mercury Assessment: Sources, Emissions and Transport, 2008.
UNEP: United Nations Environment Program, Chemicals Branch, Mercury, Time to Act, 2013.
UNEP: United Nations Environment Program: http://www.mercuryconvention.org (last access: May 2014), 2014
US EPA: United States Environmental Protection Agency "Mercury Research Strategy", EPA/600/R-00/073, September 2000.
US EPA: Memorandum: Emissions Overview: Hazardous Air Pollutants in Support of the Final Mercury and Air Toxics Standard, US EPA, EPA-454/R-11-014, available at: http://www.epa.gov/mats/pdfs/20111216EmissionsOverviewMemo.pdf (last access: May 2014), 2011.

AMTD
7, 5651–5693, 2014

Table 1. Typical detection sensitivities.

λ_2 nm	λ_{254} power mJ	λ_2 power mJ	Rep. Rate	[Hg] ng m^{-3}	Detection sensitivity (10 s) pg m^{-3}
408	0.6	4	10	2.5	30
313	1	2	10	2.5	15
313	0.7	0.2	50	2.5	35

AMTD
7, 5651–5693, 2014

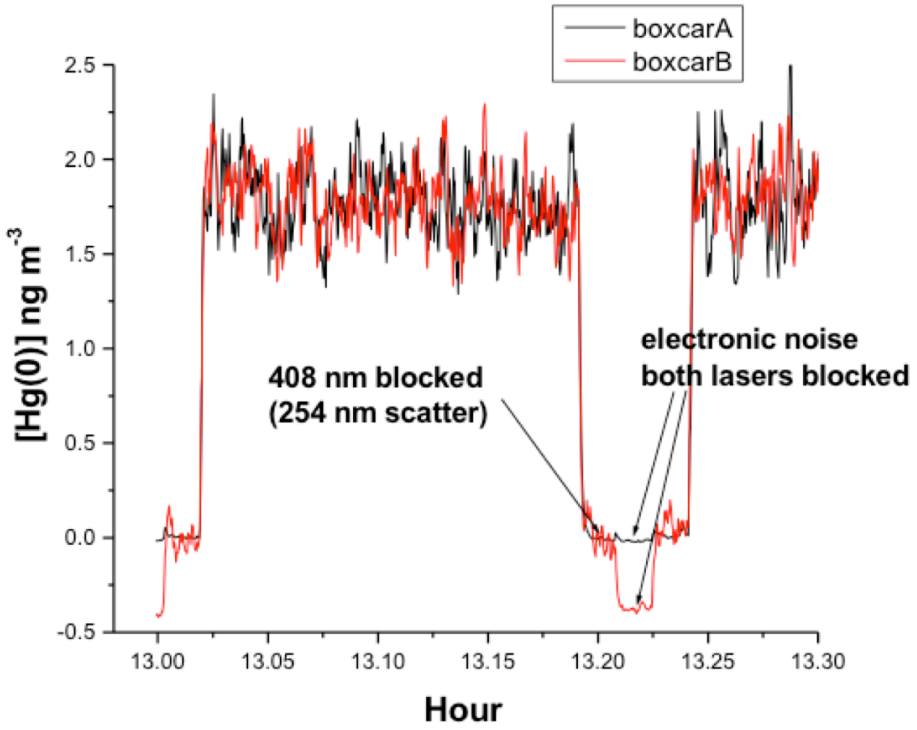

Figure 1. 2P-LIF signal from sample cell collected on 1 September from the boxcar channels (effective averaging of 70 shots at 10 Hz, i.e. 7 s). Signals from both detection PMTs are shown. The 254 nm scattered light and the electronic background noise are labeled.

AMTD
7, 5651–5693, 2014

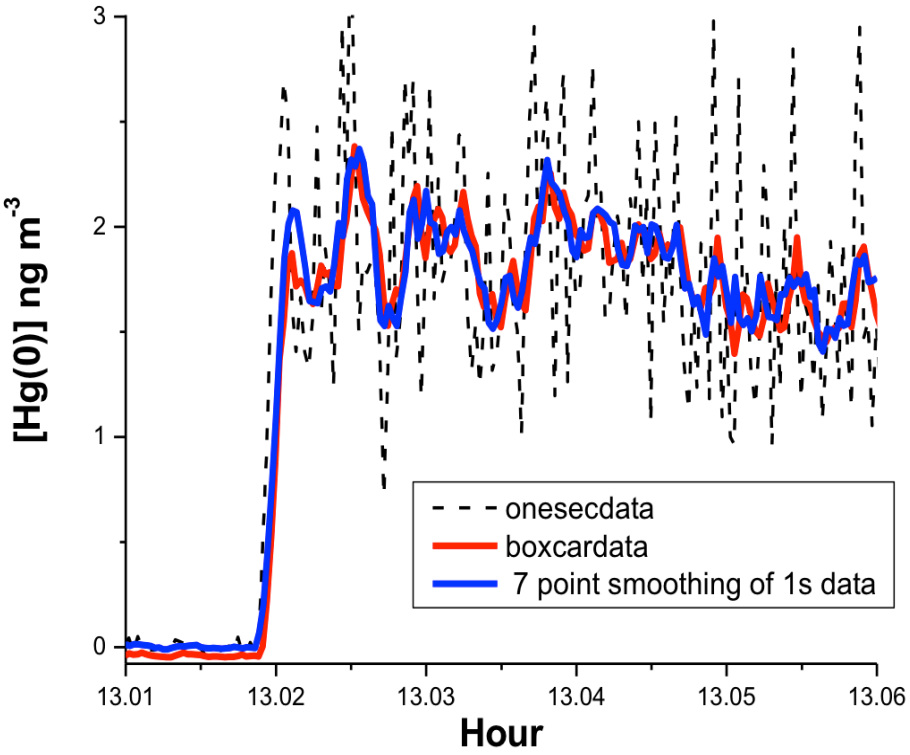

Figure 2. Comparison of 1 s average of 10 Hz data, output of boxcar averaged data, and a 7 s smoothing of the 1 s data.

AMTD
7, 5651–5693, 2014

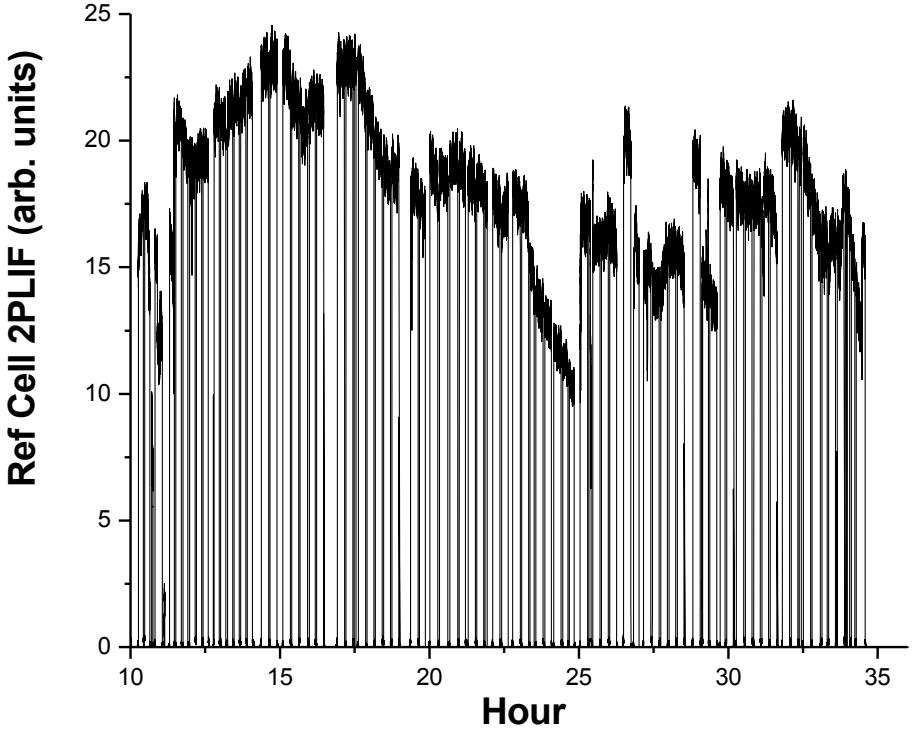

Figure 3. Reference cell signal over a 26 h sampling period on 1 and 2 September.

AMTD
7, 5651–5693, 2014

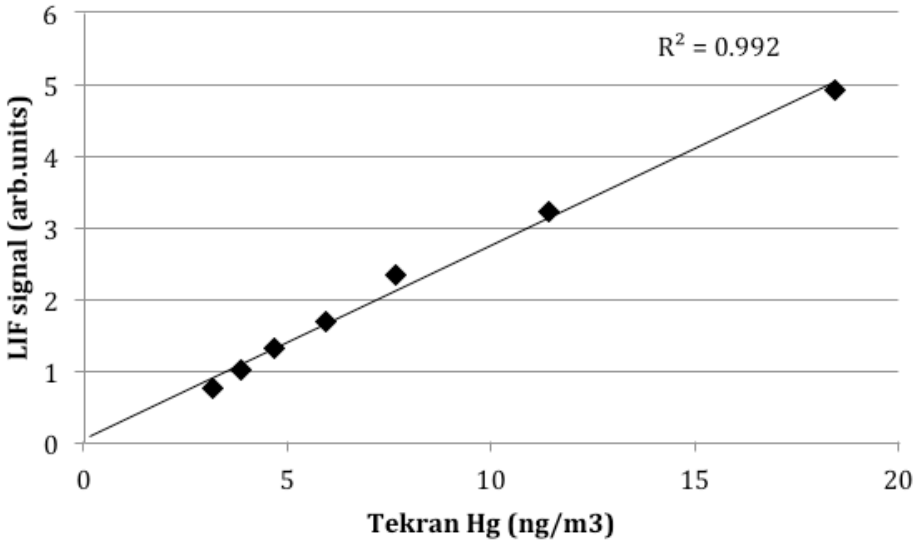

Figure 4. The 2P-LIF signal as a function of Hg(0) concentration in zero-grade air together with a calculated regression line.

AMTD
7, 5651–5693, 2014

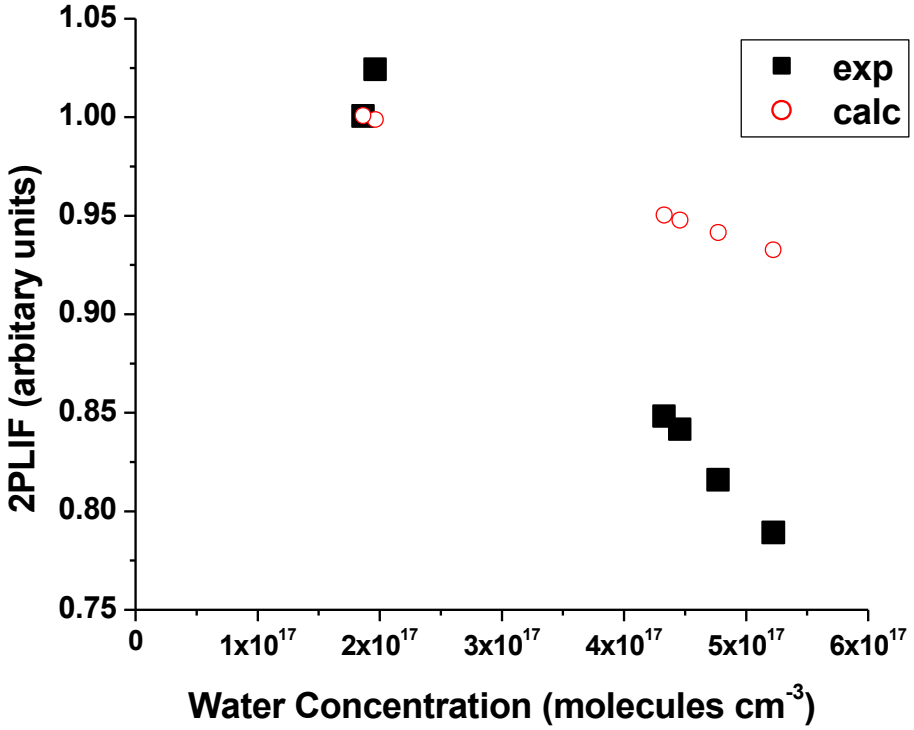

Figure 5. The 2P-LIF signal as a function of H_2O concentration. The calculated points show the expected attenuation based only on absorption of the 2P-LIF by H_2O.

AMTD
7, 5651–5693, 2014

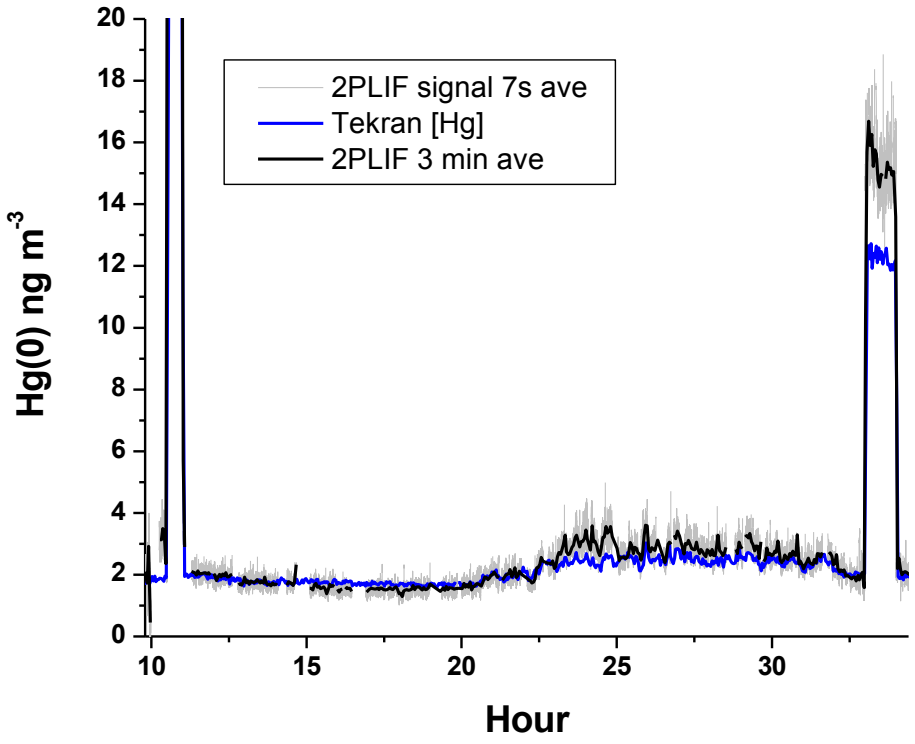

Figure 6. 2P-LIF and Tekran signals over a 26 h sampling period on 1 and 2 September. The Tekran samples every 2.5 min. The 7 s boxcar output is shown together with a 3 min smoothing of the boxcar output.

AMTD
7, 5651–5693, 2014

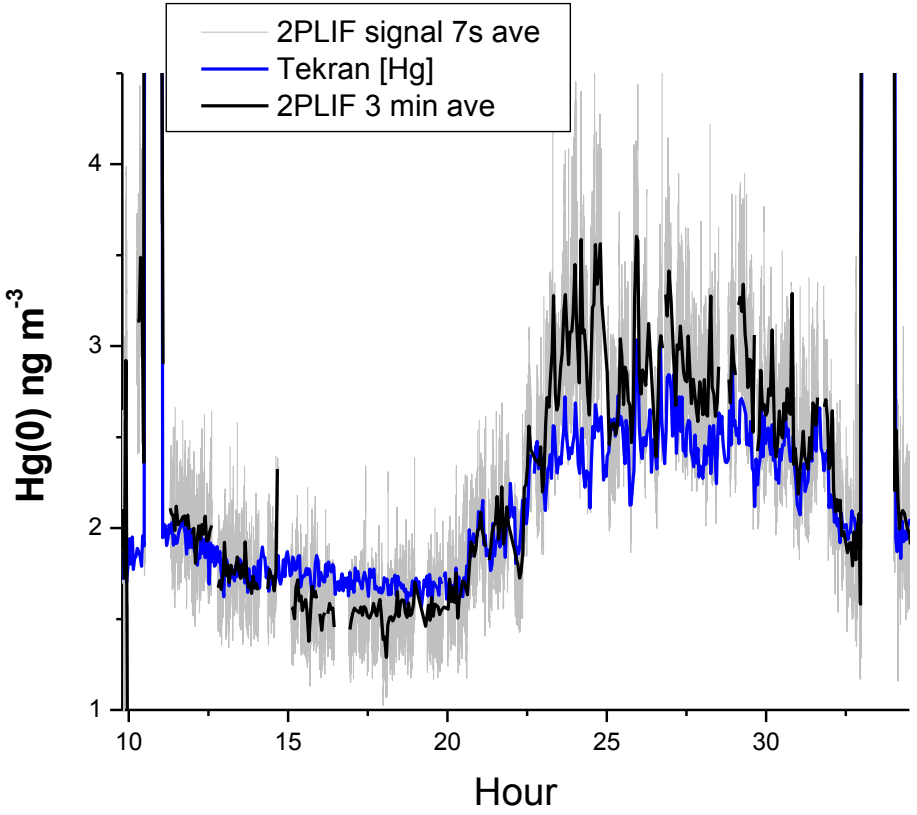

Figure 7. LIF and Tekran signals over a 26 h sampling period on 1 and 2 September. The Tekran samples every 2.5 min. The 7 s boxcar output is shown together with a 3 min smoothing of the boxcar output. The concentration scale is expanded to show the ambient data more clearly.

AMTD
7, 5651–5693, 2014

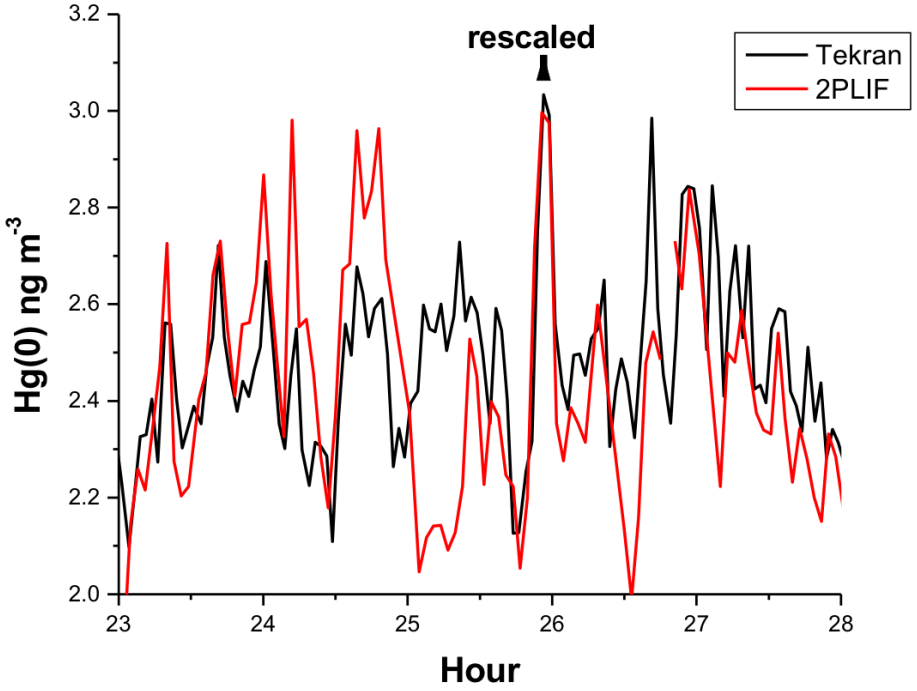

Figure 8. An expanded section of the 1–2 September sampling period showing the nighttime variation is Hg(0) detected by the Tekran and 2P-LIF instruments. The 2P-LIF data is rescaled to the labeled peak.

AMTD
7, 5651–5693, 2014

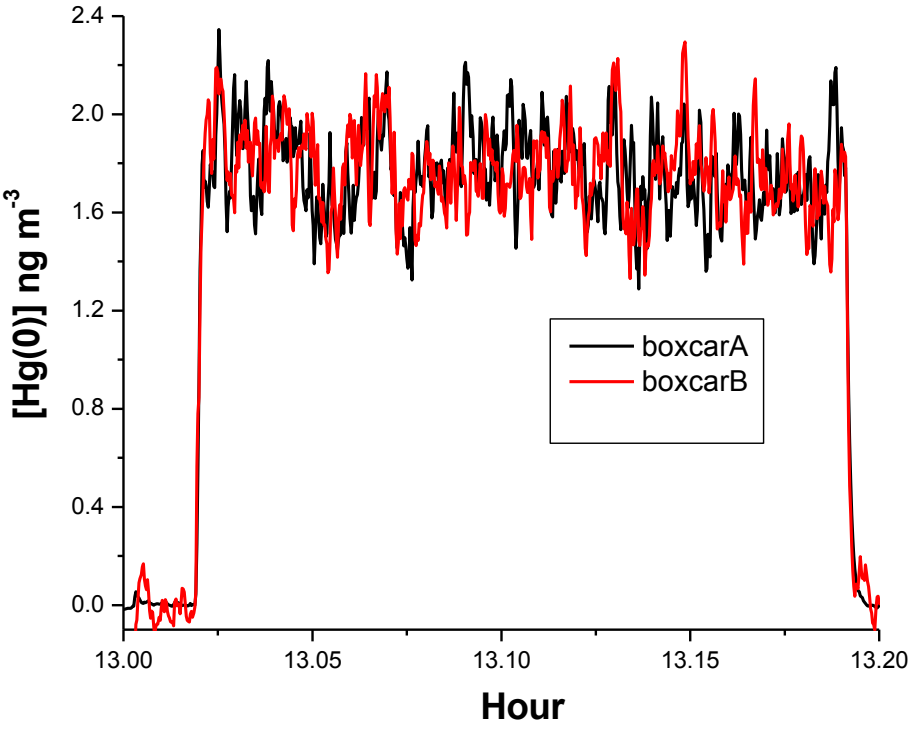

Figure 9. 2P-LIF signals from the two individual boxcar channels over a 10 min sampling period at ~ 1 p.m. LT on 1 September.

AMTD
7, 5651–5693, 2014

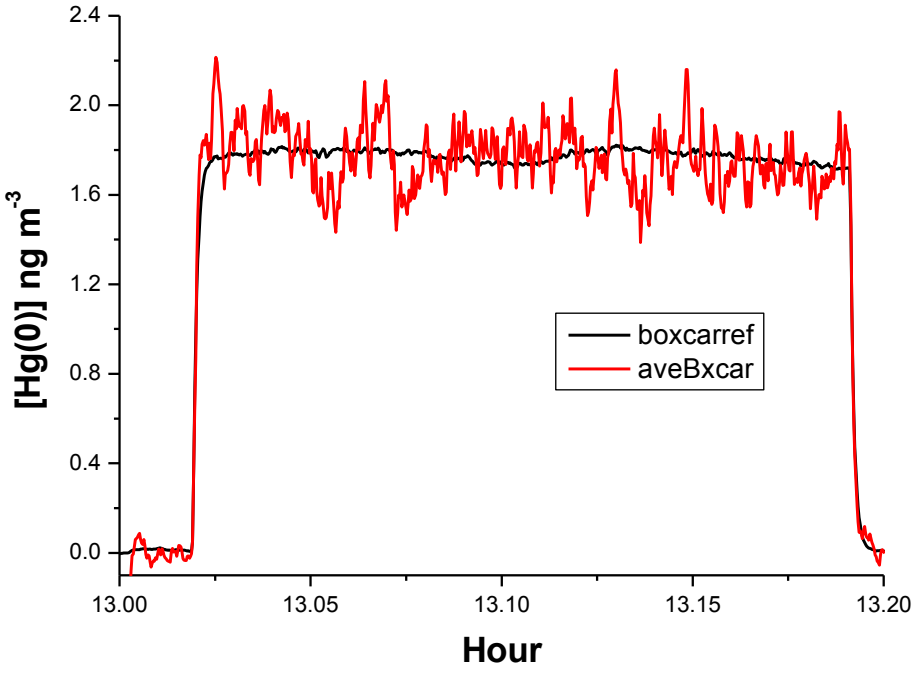

Figure 10. Average of the 2P-LIF shown in Fig. 9 together with the reference cell signal normalized to the same amplitude.

AMTD
7, 5651–5693, 2014

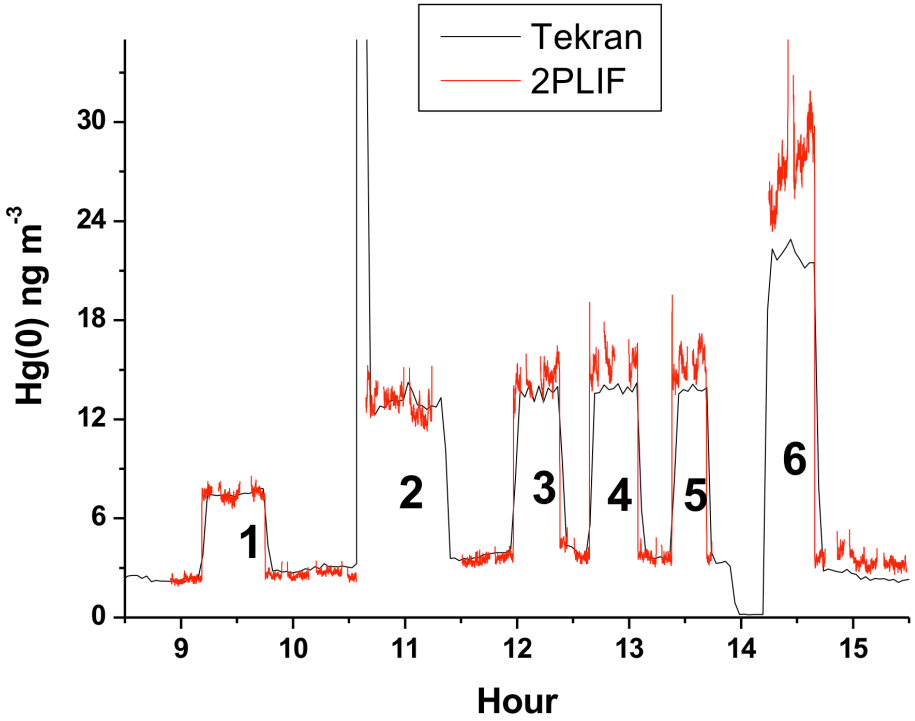

Figure 11. Data from 8 September showing ambient, manifold spike, and in-situ 2P-LIF calibration using permeation oven additions.

AMTD
7, 5651–5693, 2014

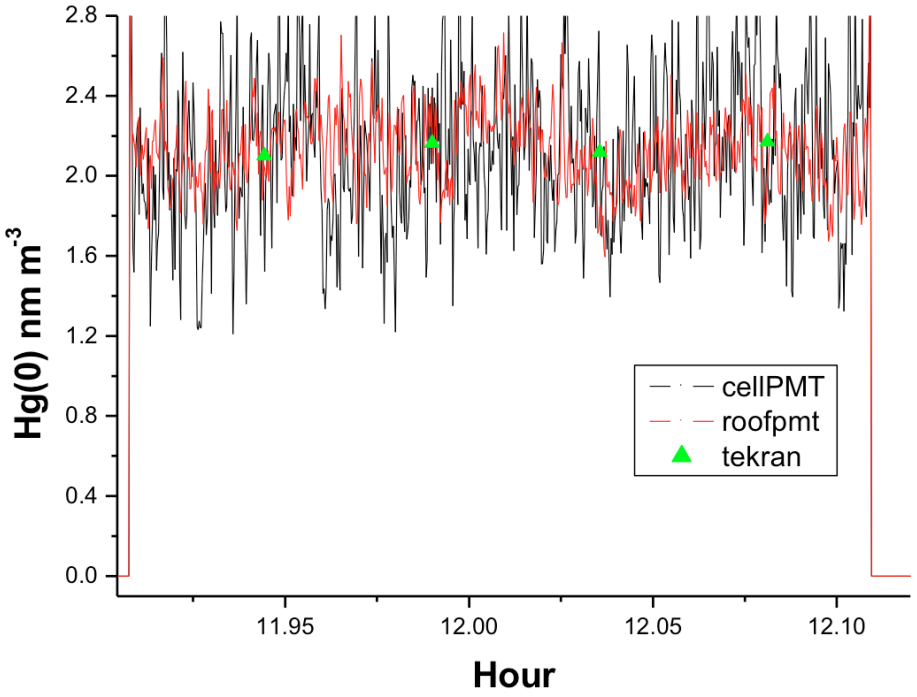

Figure 12. Comparison of 2P-LIF signals from PMTs located on the trailer roof and the sample cell. The signals are normalized to the concentrations measured by the Tekran. Data from 16 September at ~ noon.

AMTD
7, 5651–5693, 2014

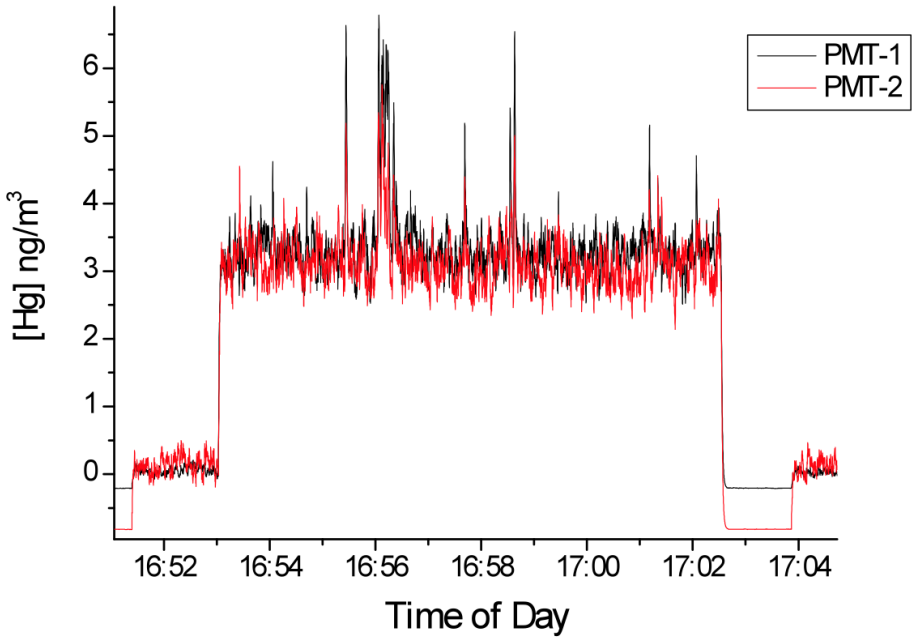

Figure 13. 2P-LIF signal from two individual boxcar channels with 254/313 nm excitation scheme using a 10 Hz laser system. The figure shows a ten-minute slice of a one-hour sample.

AMTD
7, 5651–5693, 2014

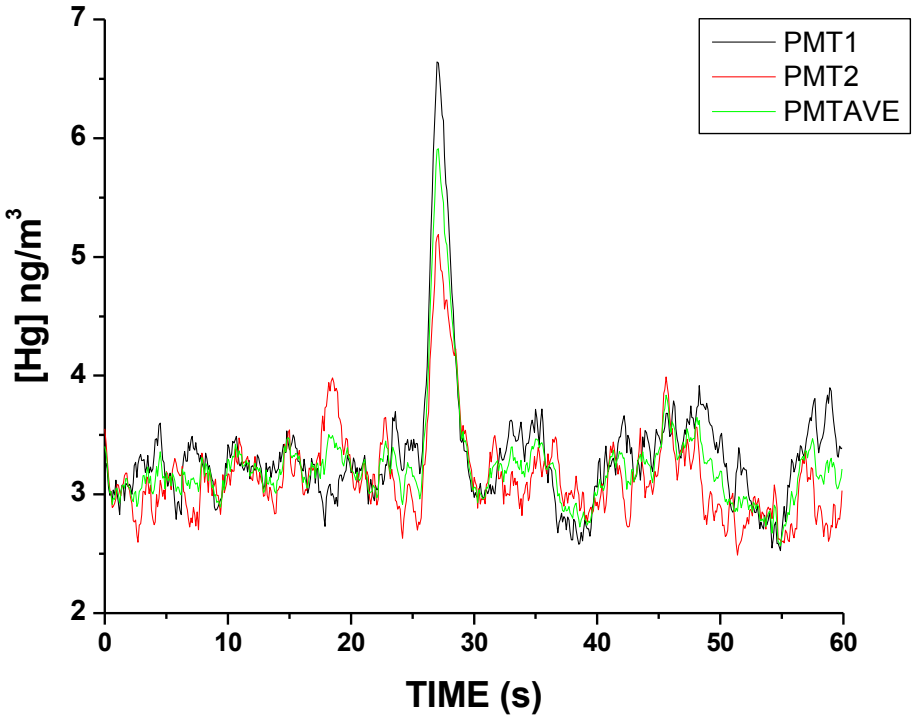

Figure 14. 2P-LIF signal with 254/313 nm excitation scheme showing a one-minute slice of a one-hour sample at specific time of hour 16.55. The individual boxcar channels and their average are shown.

AMTD
7, 5651–5693, 2014

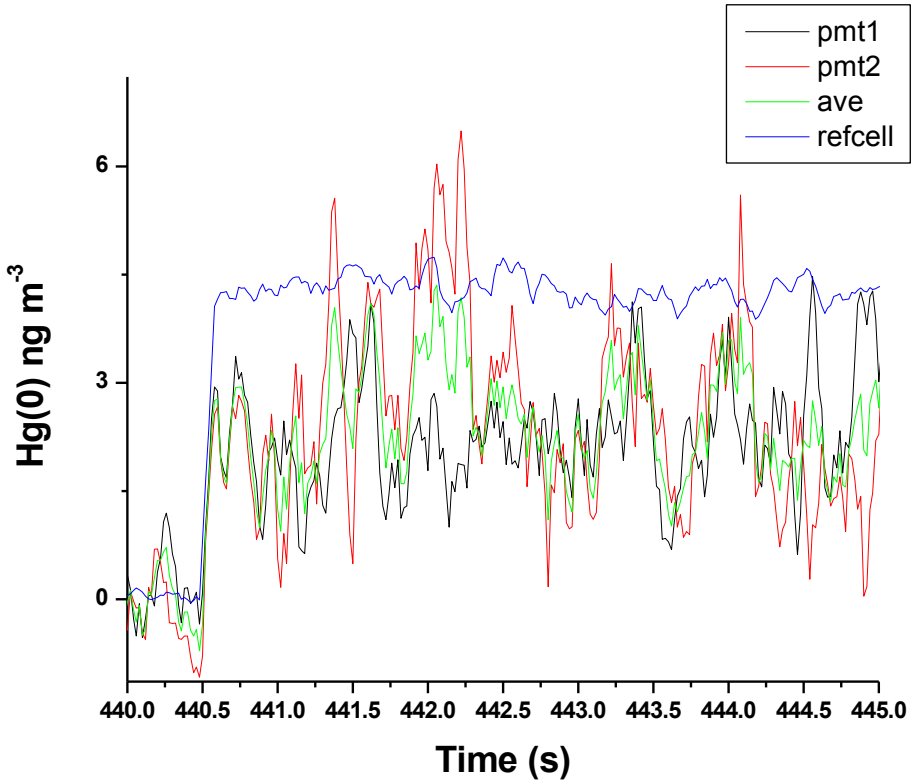

Figure 15. 2P-LIF ambient sample using 50 Hz laser system, taking 5 shot averages to give an effective sampling time of 10 Hz. The figure shows a 5 s slice of data giving the outputs of PMT A, PMT B, their average and the reference cell.

AMTD
7, 5651–5693, 2014